Applied Ocean Research xxx (2017) xxx–xxx

Contents lists available at ScienceDirect

Applied Ocean Research

journal homepage: www.elsevier.com/locate/apor

Benchmark computations for flows around a stationary cylinder with high Reynolds numbers by RANS-overset grid approach

Haixuan Ye, Decheng Wan*

State Key Laboratory of Ocean Engineering, School of Naval Architecture, Ocean and Civil Engineering, Shanghai Jiao Tong University, Collaborative Innovation Center for Advanced Ship and Deep-Sea Exploration, Shanghai 200240, China

ARTICLE INFO

Article history:
Received 26 January 2015
Received in revised form 12 August 2016
Accepted 30 October 2016
Available online xxx

Keywords:
Stationary cylinder
RANS simualtion
Overset grid
High Reynolds numbers
Benchmark computations

ABSTRACT

The aim of this paper is to evaluate the accuracy, stability and efficiency of the overset grid approach coupled with the RANS (Reynolds Averaged Navier-Stokes) model via the benchmark computations of flows around a stationary smooth circular cylinder. Two dimensional numerical results are presented within a wide range of Reynolds numbers ($6.31 \times 10^4 \sim 7.57 \times 10^5$) including the critical flow regime. All the simulations are carried out using the RANS solver *pimpleFoam* provided by OpenFOAM, an open source CFD (Computational Fluid Dynamics) toolkit. Firstly, a grid convergence study is performed. The results of the time-averaged drag and lift force coefficients, root-mean square value of lift force coefficient and Strouhal number (*St* number) are then compared with the experimental data. The velocity, vorticity fields and pressure distribution are also given. One main conclusion is that the numerical solutions in regard to a fixed cylinderare not deteriorated due to the implementation of the overset grid. Furthermore, it can be an appealing approach to facilitate simulations of Vortex Induced Vibrations (VIV), which involves grid deformation. The present study is a good start to implement the overset grid to solve VIV problems in the future.

1. Introduction

With the development of offshore oil industry in deep sea, the security of risers becomes increasingly important. As fatigue damages caused by the VIV of risers play a pivotal role in the design of the risers [1], a clear understanding of the mechanism of VIV is essential to accurately predict the dynamic responses of risers and for their optimal design. Flow past a stationary smooth cylinder is a starting point to understand the VIV phenomena.

The flow around a circular cylinder is quite complicated with the increase of Reynolds numbers regardless of its simple geometry. The complication of the flow is closely related to the boundary layer, separated and reattached shear layer and wake flow. Nowadays, these phenomena are increasingly investigated by CFD methods. Generally, there are three main trends of CFD methods, which are Direct Numerical Simulation (DNS) [2], Large Eddy Simulation (LES) [3] and RANS [4]. Direct simulations of flows past a stationary circular cylinder and a cylinder undergoing forced oscillations were performed by Dong and Karniadakis [5]. They increased the Reynolds number up to 10000 by employing a multilevel-type parallel algorithm and the physical quantities of the flows were well captured. The flows around a circular cylinder at supercritical Reynolds numbers from $5 \times 10^5 \sim 2 \times 10^6$ were investigated by Catalano et al. [6] using LES and a wall function model. The distributions of mean pressure and overall drag coefficients were predicted reasonably well at lower Reynolds numbers. However, the solutions were inaccurate at higher Reynolds numbers. Though it is widely agreed that DNS and LES can capture more details of the flow structures than RANS models, the tremendous computational cost, especially in the cases of high Reynolds numbers, makes them difficult to meet industrial demands. RANS models find a balance between the accuracy and the efficiency by properly modelling of turbulence. 2D flows past a circular cylinder for subcritical and supercritical Reynolds numbers were simulated using RANS by Saghafian et al. [7] by implementing a nonlinear eddy-viscosity model. The Strouhal number and separation position were in good agreement with the experiments, while the drag was overestimated. The 2D RANS computations of an oscillating cylinder with low mass-damping were also carried out by Guilmineau and Queutey [8]. They investigated the vortex shedding in the Reynolds number range 900–15000, and predicted the maximum amplitude of vibration. A detailed comparison between the results of RANS and experiments was conducted by Pan et al. [9]. They revealed some random characteristics of VIV responses and their influence

* Corresponding author.
E-mail address: dcwan@sjtu.edu.cn (D. Wan).

http://dx.doi.org/10.1016/j.apor.2016.10.010
0141-1187/

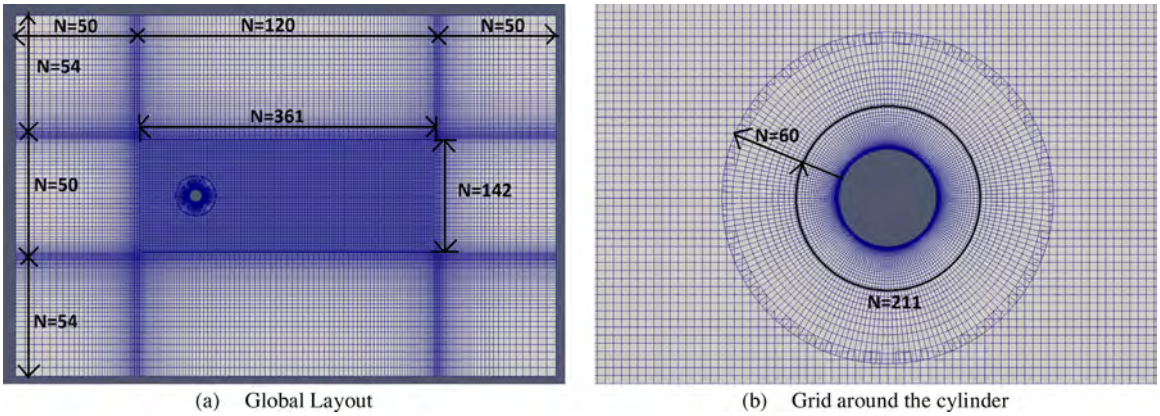

Fig. 1. Overset grid layout.

on the observations. Nowadays, Detached Eddy Simulation (DES) becomes increasingly popular. It modifies a RANS model by switching to a LES calculation in regions where the grids are fine enough and is assigned the RANS model of solution near the solid boundaries where the turbulent length scale is less than the maximum grid dimension. Thus this method can accurately predict vortex in the wake flow, and at the same time, has a relatively low amount of computational effort in the boundary layer. Travin et al. [10] calculated the flows with either laminar or turbulent separation at the surface of a circular cylinder. The paper revealed that DES was much more accurate than RANS for the cases involving laminar separation, while the results of DES and RANS were very close in the cases when turbulent separation happened.

It is well known that the quality of grid has a great influence on the numerical solutions. Although high quality structured grids can be generated easily to study the flows around a stationary cylinder, it becomes harder to preserve the quality of grids when the motions of the cylinder are considered. By contrast, the overset grid technique can be a good choice. One of its major advantage is to keep the grid quality under large motions of a cylinder. During a simulation, the shape of each component grid is kept, and the body motions are simulated depending on the relative positions of different component grids. In this way, the grid quality can be preserved regardless of the amplitude of body motions. Many researches have been conducted using overset grids [11–14].

The purpose of this paper is to implement the overset grid approach into RANS simulations and to evaluate its accuracy, stability and efficiency. Several Reynolds numbers lying in and around the critical flow regime are considered and the numerical results are compared with experiments. The present work still stays at a preliminary stage and the final goal is to study the VIV phenomena with the help of the overset grid approach. Additionally, it is worth noting that the implementation of the overset grids is not limited to coupling with RANS or any specific turbulence model or near-wall treatment. Thus, results better than the present ones can be expected if overset grid approach is used together with other advanced models which can capture the turbulent flow around the cylinder more accurately.

2. Numerical methods

2.1. Governing equations

All computations in this paper are conducted with the incompressible RANS solver *pimpleFoam*, which is provided by OpenFOAM. Eqs. (1) and (2) are the governing equations.

$$\nabla \cdot \mathbf{V} = 0 \tag{1}$$

$$\frac{\partial \rho \mathbf{V}}{\partial t} + \nabla \cdot (\rho \mathbf{V} V) = \nabla \cdot (\mu_{eff} \nabla \mathbf{V}) + (\nabla \mathbf{V}) \cdot \nabla \mu_{eff} - \nabla p \tag{2}$$

where, $\mu_{eff} = \rho(\nu - \nu_t)$ is the effective dynamic viscosity, in which ν_t is obtained from the turbulence model, which is the *k-ω SST* turbulence model [15] in this paper.

2.2. Turbulence modelling

The *k-ω SST* turbulence model by Menter [15] is employed. It combines the advantages of the *k-ω SST* turbulence model for the free-stream flow and the standard *k-ω* turbulence model for the boundary layer flow. The *SST* turbulence model employed in OpenFOAM v2.0.1 is based on a blend of high Reynolds number versions of *k-ε* and *k-ω* turbulence models [16]. It implies that the *SST* model is based on the assumption that the flow field is fully turbulent, and therefore the turbulence model has no damping functions for low Reynolds number flows. However, as for the Reynolds numbers considered in this paper, the boundary layer on the surface of the cylinder transits from laminar to turbulent [17]. Thus, proper wall functions are needed for the turbulence kinetic energy *k*, specific turbulence dissipation ω and turbulent viscosity ν_t to improve the numerical results.

2.3. Near-wall treatments

For the turbulence kinetic energy *k*, the *kqRWallFunction* boundary condition is implemented, which is a zero-gradient condition of *k*.

For the specific turbulence dissipation ω, the *omegaWallFunction* boundary condition s is used and expressed as Eq. (3).

$$\omega = \sqrt{\omega_{vis}^2 + \omega_{log}^2} \tag{3}$$

in which, ω_{vis} and ω_{log} are ω in viscous and logarithmic regions, respectively. $\omega_{vis}$and ω_{log} are expressed as Eq. (4).

$$\omega_{vis} = \frac{6\nu}{0.075(y^+)^2}; \qquad \omega_{log} = \frac{1}{0.3\kappa}\frac{u_\tau}{y^+} \tag{4}$$

For the turbulent viscosity ν_t, the *nutUSpaldingWallFunction* is chosen. It gives a continuous ν_t profile to the wall according to Spalding's law [11] as Eq. (5).

$$y^+ = u^+ + \frac{1}{9.8}\left[e^{\kappa u^+} - 1 - \kappa u^+ - 0.5(\kappa u^+)^2 - \frac{1}{6}(\kappa u^+)^3\right] \tag{5}$$

where κ is Von Karman constant.

Please cite this article in press as: H. Ye, D. Wan, Benchmark computations for flows around a stationary cylinder with high Reynolds numbers by RANS-overset grid approach, Applied Ocean Research (2017), http://dx.doi.org/10.1016/j.apor.2016.10.010

2.4. Overset grid approach

The implementation of the overset grid approach is composed of two main steps: (1) generating the communicating information between different component grids, and (2) executing the flow solver *pimpleFoam* using the information obtained from step (1). Both steps are discussed further as below.

To generate the communicating information requires three substeps. Take the grids in the current work as an example. Three component grids, a background block, a block around the cylinder and a transition block, are needed. Firstly, grid cells lying inside the cylinder, namely outside the computational domain, are marked as invalid ones (hole cells); Secondly, grid cells lying inside the overlapping region between the background and the transition block or between the transition block and the block around the cylinder are identified as either donors or fringes depending on the flow direction of information. Specifically, donor cells provide information used for interpolation. The velocity, pressure and turbulent variables at the fringe cells are obtained from the interpolation of the donors. Finally, the interpolation stencils for all blocks are generated to determine how to communicate between the blocks. An interpolation stencil is a list of interpolation weights η and corresponding relation between fringes and their donors. The interpolating process of any flow variable ϕ can be expressed as Eq. (6).

$$\phi = \sum_{i=1} \eta_i \phi_i \tag{6}$$

in which, ϕ is any flow variable at a fringe cell. ϕ_i and η_i is the flow variable and the corresponding interpolation weight at the i^{th} donor cell of the fringe cell.

After the interpolation stencils are generated, they are used when solving the flow field. Specifically, they are used to assemble the linear algebraic equations in different blocks of grids into a large one. That the cylinder is fixed in the current work means the interpolation stencils are generated only one time before the flow field is solved. If the motions of the cylinder are considered, however, stencils should be updated in each time step. To implement overset grids in *pimpleFoam*, new classes are written within the code frame of OpenFOAM. The interpolation of any flow variable can be achieved by calling the member functions of the new classes. It should be noted that this overset gird approach can be implemented in not only *pimpleFoam* but also any other solver provided by OpenFOAM.

2.5. Numerical schemes

The scheme is the first-order implicit Euler scheme [18] for temporal discretization, and the first-order upwind scheme for the convection term. The discretization scheme for the diffusion term is the second-order central differencing scheme with a coefficient $\Phi = 0.5$ taking into account the non-orthogonal correction of the grids. PIMPLE, which is a combination of SIMPLE [19] and PISO [20] is employed to decoupling the velocity and pressure. Each time step includes several iterations of SIMPLE taking the flow field as a steady one due to small time step. The PISO algorithm is then used to advance the time steps treating the flow field as unsteady. The linear solver for all flow variables is the overset-version of Geometric Agglomerated Algebraic Multigrid (GAMG) [21] solver.

3. Cases setup

Flows around a fixed smooth circular cylinder are studied in this paper. The cylinder has a diameter $d = 0.206$m, which is consistent with the experiments by Wilde et al. [22]. All the computations are 2D ones neglecting all 3D effects. The diameter of the cylinder is chosen as the characteristic length and the Reynolds number Re_d is defined as Eq. (7).

$$Re_d = \frac{\rho V_{in} d}{\mu} \tag{7}$$

in which, ρ is the water density, V_{in} is the horizontal component of the upstream velocity and μ is the water viscosity.

Six Reynolds number 6.31×10^4, 1.26×10^5, 2.52×10^5, 3.15×10^5, 5.06×10^5, 7.57×10^5 are considered which are in and around the critical flow regime. For all cases, time steps are chosen to make sure that the Courant number is less than 0.5. In addition, the residual criterions of all physical quantities are set to be 1e-3.

Fig. 1 shows the grid layout and the size of the computational domain, in which N is the number of grid nodes. Three grid components are used, which are a block around the cylinder, a transition block and a background block. The transition and background blocks are completely orthogonal. In all cases, the dimensionless wall distance y^+ is constrained between 1 and 5. The block around the cylinder and the transition block are refined to capture the flow features near the cylinder and in the wake. The background block is coarsened to decrease the total number of grid cells. In Fig. 1(a), the flow direction is from left to right. The flow velocity V_{in} is specified as the inlet boundary according to the Reynolds number, and the outflow boundary condition is used at the outlet boundary. Symmetry boundary condition is assigned to the upper and lower boundaries.

Specifications of the block around the cylinder and the total cell number are listed in Table 1, in which N_c and N_t represent the number of nodes in the circumferential and wall normal direction of the cylinder in the block around the cylinder. The N_t increases slightly with the Reynolds number increasing to obtain the proper y^+.

Except the cases using the overset gird approach, ones without using the approach are also conducted for comparison, in which all numerical schemes are kept the same as in the cases using overset grids. The layout of the grids is shown in Fig. 2. For cases without

Table 1
Grids around the cylinder.

Re_d	N_c	N_t	Total cell numbers
6.31×10^4	211	60	96785
1.25×10^5	211	60	96785
2.52×10^5	211	60	96785
3.15×10^5	211	65	97835
5.06×10^5	211	70	98885
7.57×10^5	211	70	98885

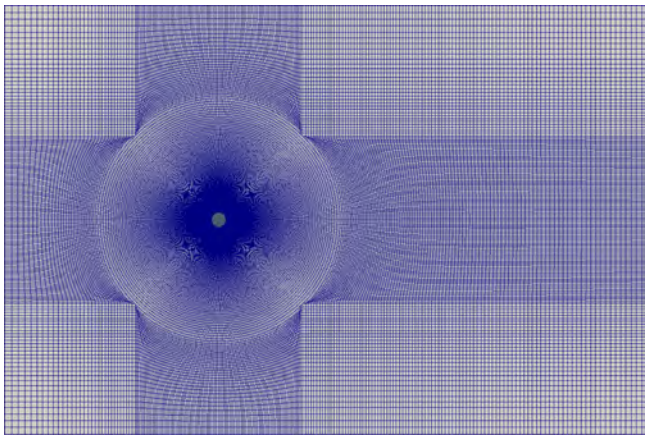

Fig. 2. Layout of the grid without overset.

Please cite this article in press as: H. Ye, D. Wan, Benchmark computations for flows around a stationary cylinder with high Reynolds numbers by RANS-overset grid approach, Applied Ocean Research (2017), http://dx.doi.org/10.1016/j.apor.2016.10.010

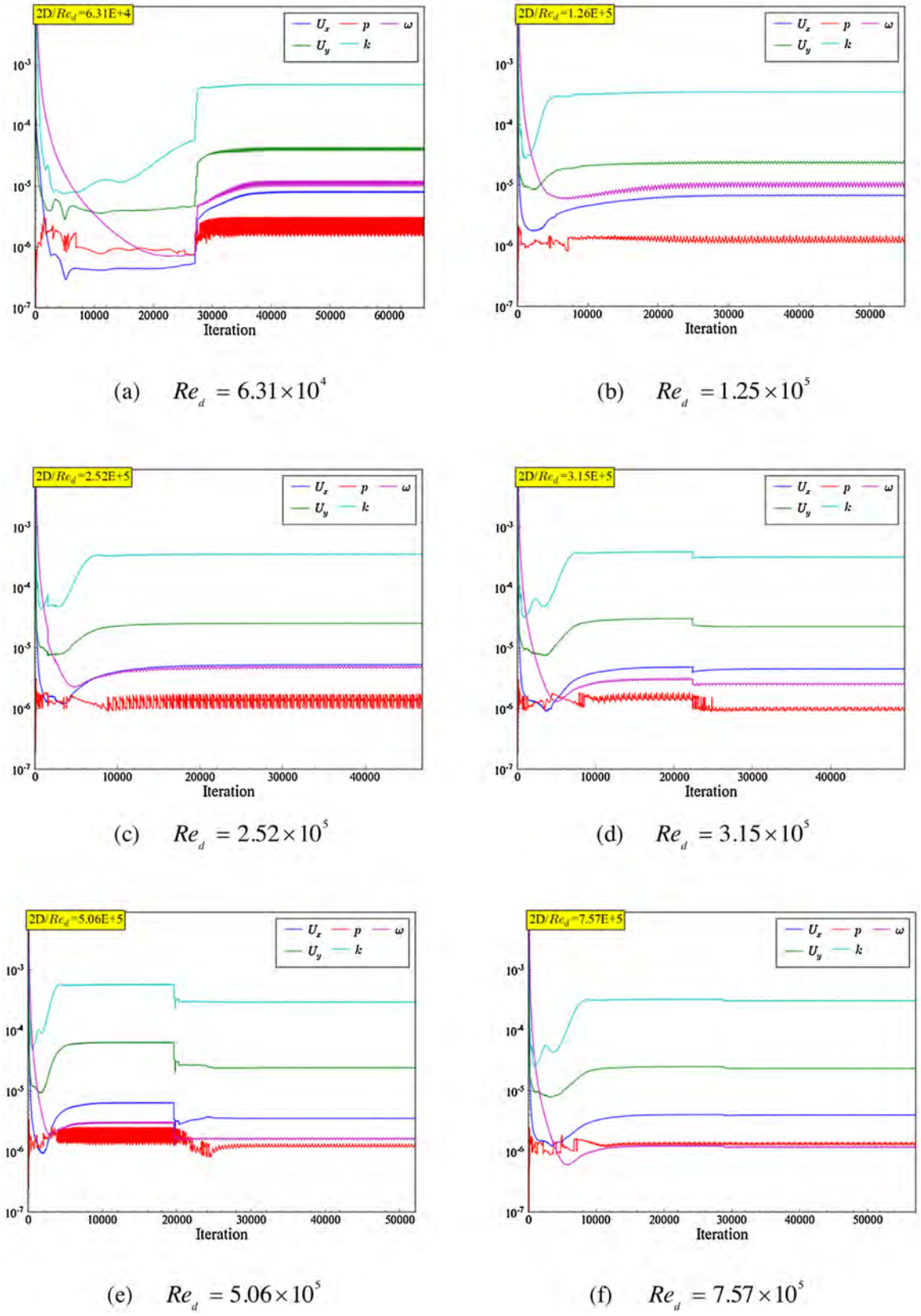

Fig. 3. Time history of residuals at different Re_d.

overset grids, a grid convergence study is also carried out at first as a spatial verification using 4 sets of grids. Due to space constraints, only the final result that are used in this paper will be presented. The result is obtained by using the third finest grid, in which N_c and N_t are 270 and 102, respectively. The total cell number is 0.137 million.

Please cite this article in press as: H. Ye, D. Wan, Benchmark computations for flows around a stationary cylinder with high Reynolds numbers by RANS-overset grid approach, Applied Ocean Research (2017), http://dx.doi.org/10.1016/j.apor.2016.10.010

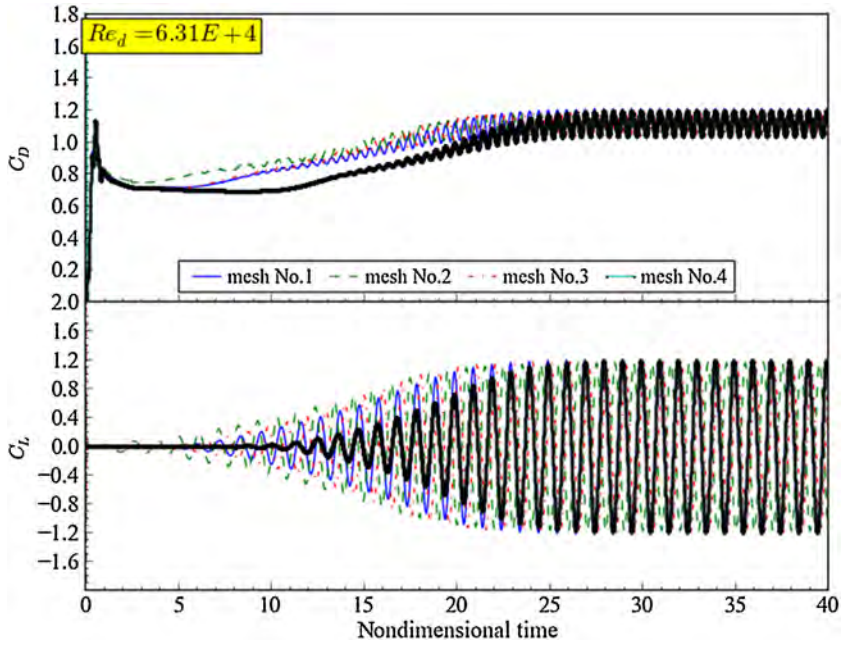

Fig. 4. Time histories of C_D and C_L in the grid convergence study.

Table 2
Grids for grid convergence study.

Grid No.	1	2	3	4
N_c	177	211	251	299
N_t	50	60	71	84
Transition	35636	50760	72072	102200
Background	23478	33635	48100	67980
Total	67738	96785	137672	194914

Table 3
Results of the grid convergence study.

Grid No.	$C_{D,ave}$	$C_{L,ave}$	$C_{L,rms}$	St
1	1.1369	0.0077	0.8635	0.2372
2	1.1157	0.0053	0.8285	0.2385
3	1.1163	0.0044	0.8378	0.2385
4	1.1191	0.0019	0.8459	0.2394
MARIN	1.16	0.0145	0.24	0.19

4. Numerical results

4.1. Grid convergence study

For cases with overset grids, a grid convergence study is conducted first using 4 sets of grids at $Re_d = 6.31 \times 10^4$. The grid specifications are listed in Table 2.

The drag coefficient C_D, lift coefficient C_L and Strouhal number St are investigated in this paper and their definitions are shown in Eq. (8).

$$C_D = \frac{F_D}{0.5\rho V_{in}^2 A}; \quad C_L = \frac{F_L}{0.5\rho V_{in}^2 A}; \quad St = \frac{f_s d}{V_{in}} \tag{8}$$

in which, F_D and F_L are the drag and lift forces, respectively. $A = d$ is the projected area of a 2D cylinder. f_s is the vortex-shedding frequency.

Table 3 presents the results of grid convergence study, including the time-averaged values of C_D and C_L, root mean square (rms) of C_L and St.

In Table 3, the experimental results are also given as a comparison. The convergence conditions of $C_{D,ave}$, $C_{L,rms}$ and St are acceptable. Whereas, $C_{L,ave}$ does not show satisfying convergence. This is mainly due to its small magnitude which makes $C_{L,ave}$ very sensitive to numerical errors. But the value of $C_{L,ave}$ tends to be zero with refining the grids. For the variables in Table 3, the deviation between the result of the coarsest grid and that of the other ones is large. It is because the poor resolution of the coarsest grid fails to capture important flow features. In comparison, the results of the other three grids are very close.

From Table 3 we can conclude $C_{D,ave}$, $C_{L,rms}$ and St converge with refining the grid. However, $C_{L,ave}$ does not show a convergence behavior. Besides, the seemingly best performance of the coarsest grid requires further investigation. It cannot indicate that the coarsest grid is the most effective one.

Fig. 3 shows the residual history of all physical quantities. All other cases show similar converging process and residuals lower than 1e-3 are achieved by all physical quantities. The sudden changes of the residuals in some cases are due to a sudden interruption of power supply of the computing cluster.

Fig. 4 shows the time historical curves of C_D and C_L for all grids. Time is nondimensionalized by the vortex-shedding period $1/f_s$. It demonstrates that C_D and C_L reach cyclic steady-state convergence in all four cases.

Considering a balance of accuracy and computational efficiency, the second set of grid in Table 2 is selected for all cases. The number of nodes in the circumferential direction of the cylinder in the block around the cylinder is slightly increased as mentioned before. The other two blocks of grids are kept the same in all cases.

4.2. $C_{D,ave}$, $C_{L,ave}$, $C_{L,rms}$ and St

Fig. 5 presents the time histories of drag and lift coefficients at all Re numbers. From the time histories of drag coefficients we can clearly see the drop of drag at the critical Re number. This phenomenon will be further analyzed later. The lift coefficient also has a very different behavior in different flow regimes. In the subcritical and supercritical flow regimes, the amplitude of C_L is not sensitive to the change of the Reynolds number. However, in the transition regime between subcritical and critical regimes, a significant drop in the amplitude of C_L can be observed.

Please cite this article in press as: H. Ye, D. Wan, Benchmark computations for flows around a stationary cylinder with high Reynolds numbers by RANS-overset grid approach, Applied Ocean Research (2017), http://dx.doi.org/10.1016/j.apor.2016.10.010

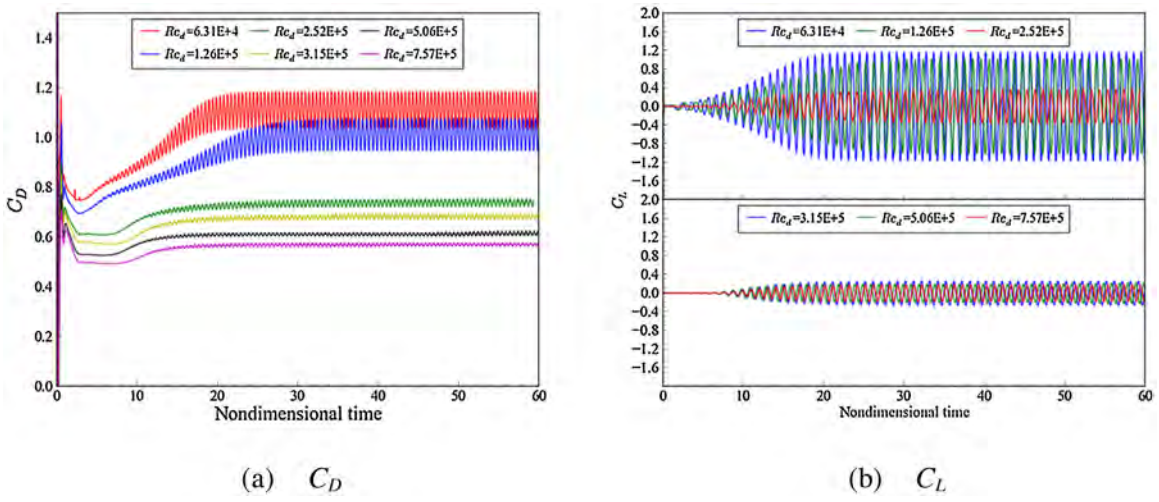

Fig. 5. Time histories of C_D and C_L at different Re_d.

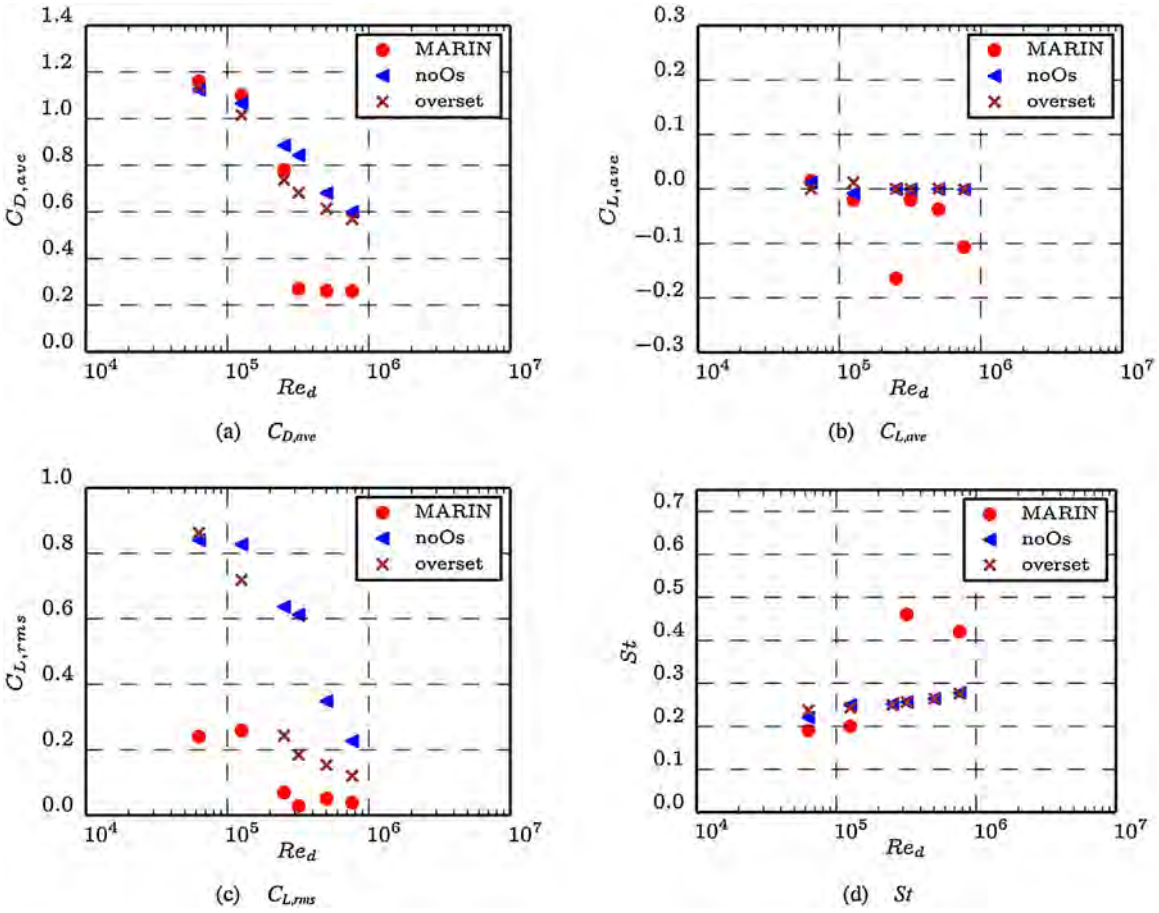

Fig. 6. Comparisons of $C_{D,ave}$, $C_{L,ave}$, $C_{L,rms}$ and St at different Re_d.

Fig. 6 presents the results of different cases. We also conduct the computations without overset grids. Computations with and without overset grids are labeled as "*overset*" and "*noOs*", respectively. In Fig. 6 are also experimental results by Wilde.

The range of Reynolds numbers covers the subcritical, critical and supercritical flow regimes. In Fig. 6(a), the drag-crisis phenomenon (when Re_d reaches $3.0\sim3.5\times10^5$) revealed by experiments is not quantitatively predicted by the RANS simulation. Although the RANS method averages the flow velocity, the decrease of drag can still be reflected from the change of mean flow velocity. Moreover, numerical computations show that the *SST* model is capable to capture flow separation to some degree [23–33]. But at the same time, it may fail to predict where the separation starts. Both of these two reasons lead to results that current computations can only predict the trend of the drag-crisis but not predict quantitatively. The numerical results only capture a decreasing trend of the drag in the critical regime. That "*overset*" and "*noOs*" obtain similar results indicates that the implementation of the

Please cite this article in press as: H. Ye, D. Wan, Benchmark computations for flows around a stationary cylinder with high Reynolds numbers by RANS-overset grid approach, Applied Ocean Research (2017), http://dx.doi.org/10.1016/j.apor.2016.10.010

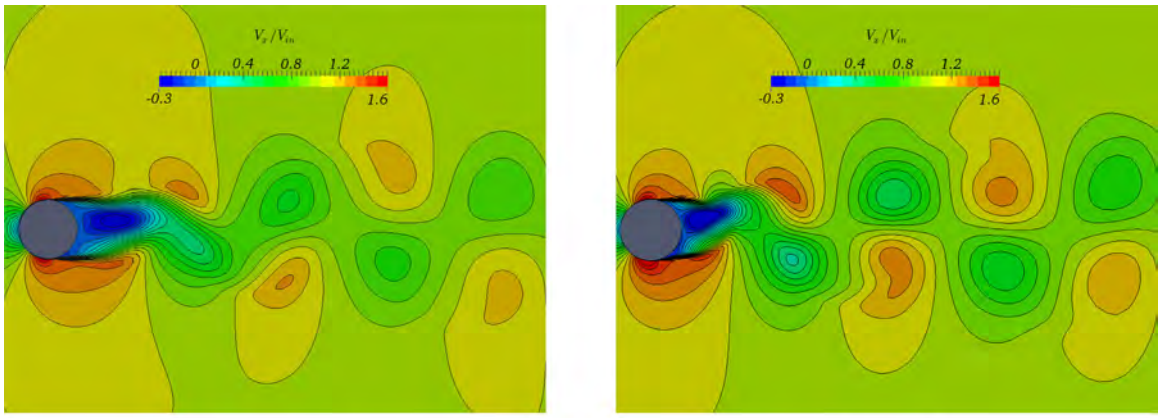

Fig. 7. V_x/V_{in} for $\theta = 0$ at $Re_d = 3.15 \times 10^5$.

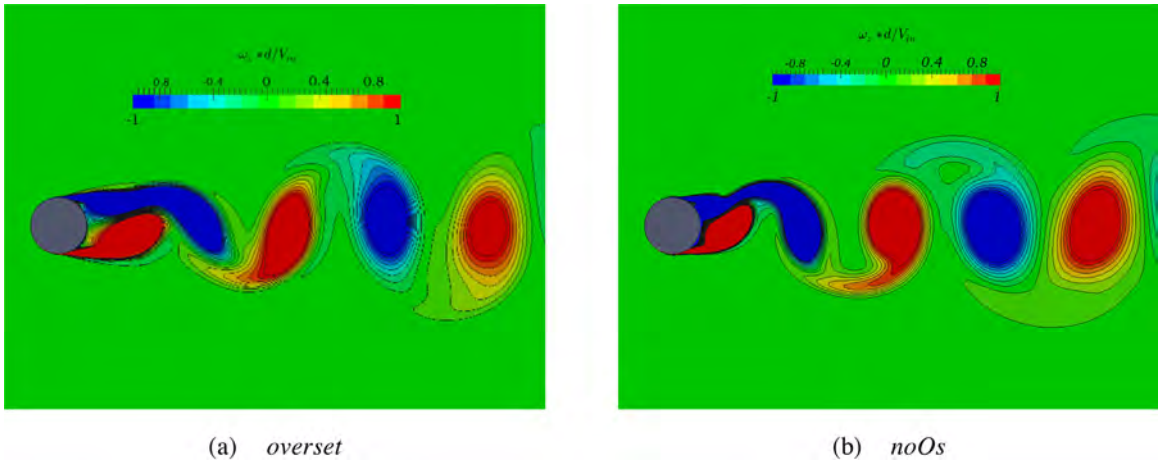

Fig. 8. $\omega_z d/V_{in}$ for $\theta = 0$ at x'.

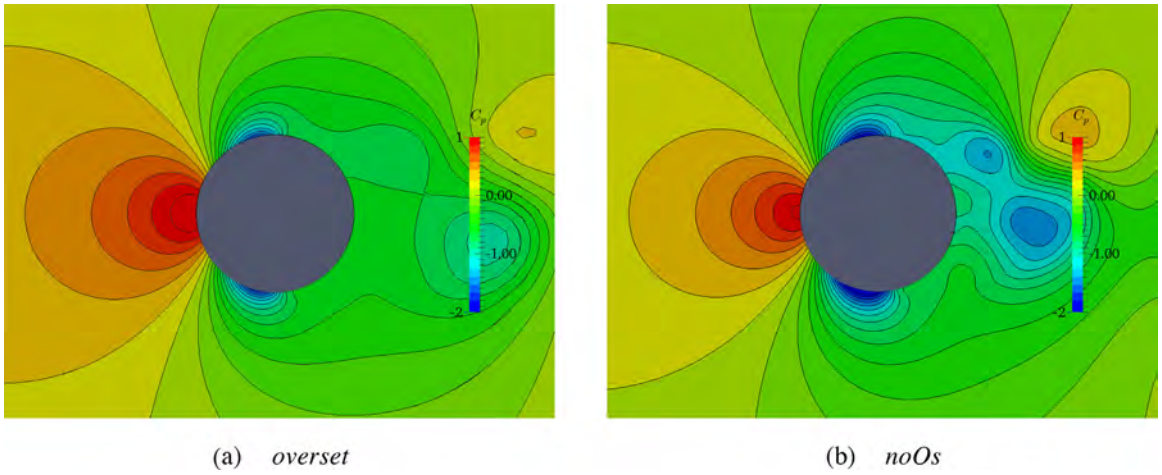

Fig. 9. C_P for $\theta = 0$ at $Re_d = 3.15 \times 10^5$.

overset grid does not violate the numerical solutions. Moreover, when $Re_d = 2.52 \times 10^5$, which is between the subcritical and critical flow regimes, "*overset*" obtained a slightly better result than that of "*noOs*". It is also noted that the present numerical schemes perform better in the subcritical flow regime than in the supercritical flow regime.

In Fig. 6(b), as the experimental data shows, a large negative value of $C_{L,ave}$ appears at the critical Reynolds number. It also indicates that in the supercritical regime, the value of $C_{L,ave}$ turns smaller with the increase of Re_d. However, neither of the numerical solutions predicts the change of $C_{L,ave}$ successfully. This may be because that the turbulence model generates superfluous eddy

Please cite this article in press as: H. Ye, D. Wan, Benchmark computations for flows around a stationary cylinder with high Reynolds numbers by RANS-overset grid approach, Applied Ocean Research (2017), http://dx.doi.org/10.1016/j.apor.2016.10.010

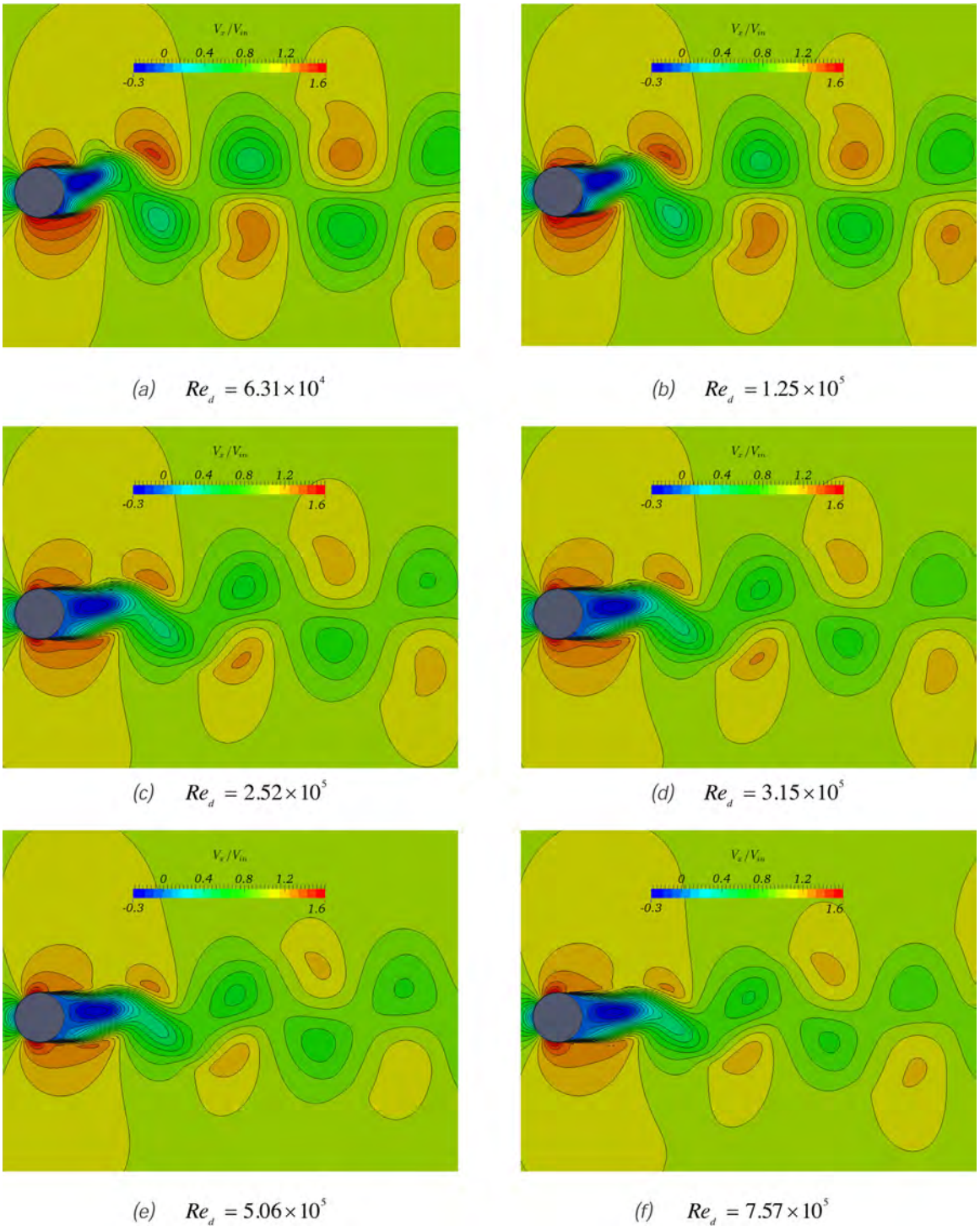

Fig. 10. V_x/V_{in} for $\theta = 0$ by overset.

viscosity dampening out some unsteadiness. Thus, it can further indicate that the *k-ω SST* turbulence model is dissipative.

The effect of instability of the separated shear layer in the critical flow regime can also be observed in Fig. 6(c). According to the experimental results, the intensity of the fluctuation of C_L decreases sharply round the critical Reynolds number, and remains low in the supercritical flow regime. The computational result captures the downward trend but the magnitude is overestimated at all Reynolds numbers. It should also be noted that "*noOs*" and "*overset*" obtain similar results in the subcritical flow regime. The similar results indicate that the overestimation of $C_{L,rms}$ is not due to the implementation of overset grids. In the supercritical flow regime, "*overset*" obtains better results than those of "*noOs*". The large deviation between the results of "*overset*" and "*noOs*" at this Reynolds number requires further investigations.

In Fig. 6(d), the computational result predicts *St* number with a satisfying accuracy in the subcritical flow regime. However, both "*overset*" and "*noOs*" fail to predict both the sharp increase of *St* number at the critical Reynolds number and its relatively large magnitude in the supercritical regime. The discrepancy between

Please cite this article in press as: H. Ye, D. Wan, Benchmark computations for flows around a stationary cylinder with high Reynolds numbers by RANS-overset grid approach, Applied Ocean Research (2017), http://dx.doi.org/10.1016/j.apor.2016.10.010

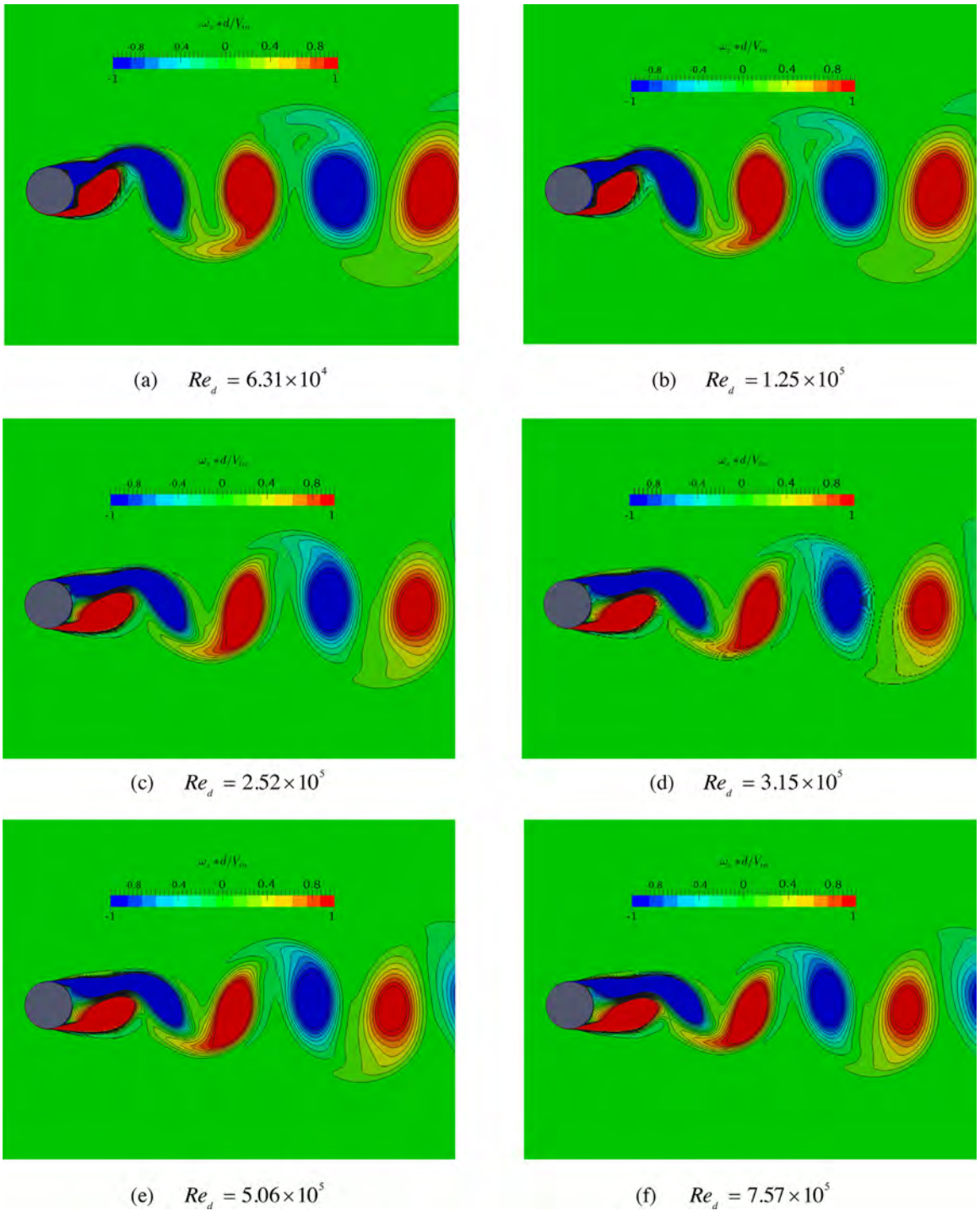

Fig. 11. $\omega_z d/V_{in}$ for $\theta = 0$ by overset.

the results of "*overset*" and "*noOs*" is very limited, which justifies that the implementation of overset grids does not have a negative influence on the prediction of *St* number.

In general, the implementation of overset grids does not deteriorate the numerical accuracy or stability for all Reynolds numbers investigated in this paper. In the supercritical flow regime, the overset grid approach slightly improved the results of $C_{L,rms}$. It should also be noted that the results of "*noOs*" and "*overset*" are close, but the total cell number of "*noOs*" is about 1.4 times as large as that of "*overset*". It proves one advantage of the overset grid approach that it can easily generate high quality grids with relatively less grid cells. Moreover, the overset gird approach combines with the numerical schemes chosen in this paper has a satisfying accuracy for predicting $C_{D,ave}$, $C_{L,ave}$ and *St* in the subcritical flow regime. The $C_{L,rms}$ predicted by "*overset*" are slightly better than those by "*noOs*" in the supercritical flow regime, but the $C_{L,rms}$ is still overall overestimated at all Re_d. It is promising to use this overset grid approach together with more advanced turbulence models to predict the flow characteristics more accurately in the critical and supercritical flow regimes.

Please cite this article in press as: H. Ye, D. Wan, Benchmark computations for flows around a stationary cylinder with high Reynolds numbers by RANS-overset grid approach, Applied Ocean Research (2017), http://dx.doi.org/10.1016/j.apor.2016.10.010

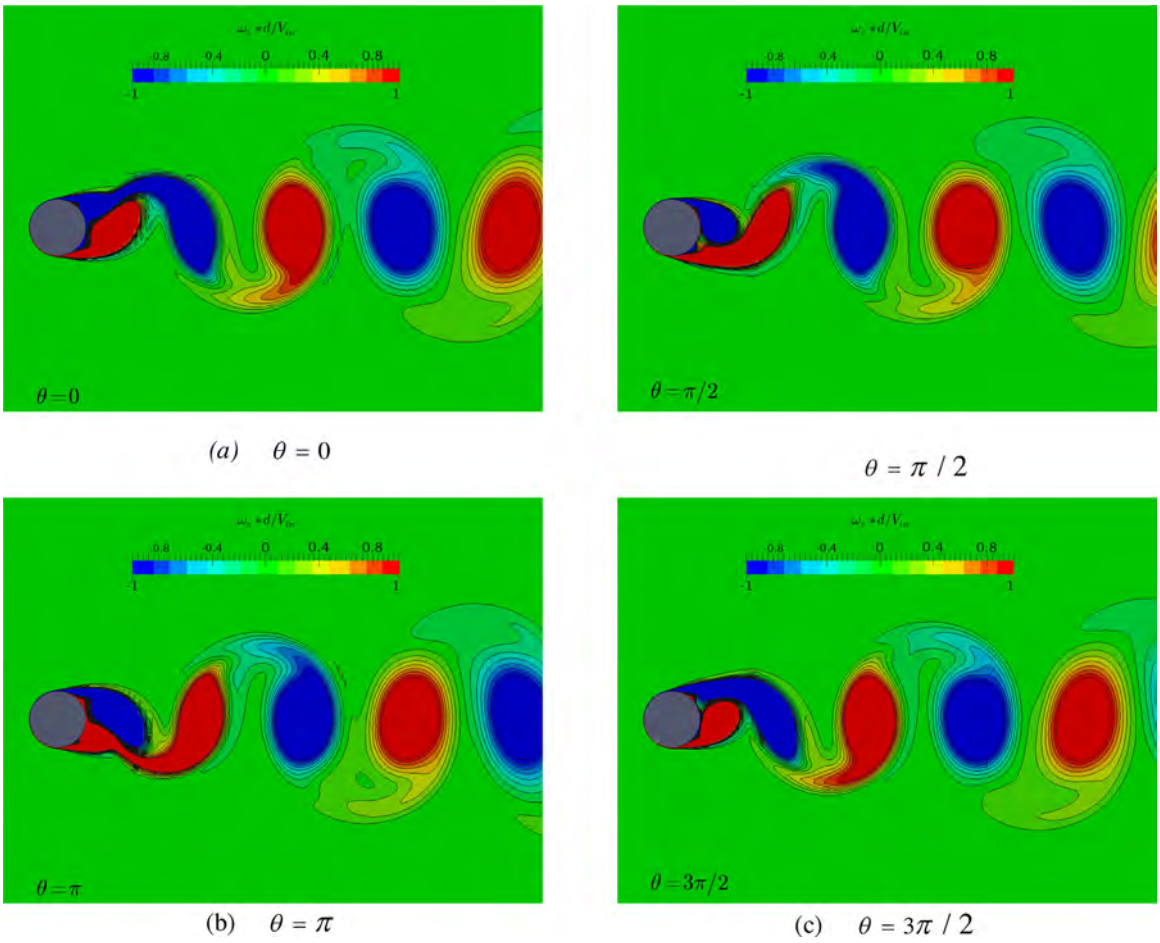

Fig. 12. $\omega_z d/V_{in}$ in a vortex-shedding period at $Re_d = 6.31 \times 10^4$ by overset.

4.3. Velocities, vorticities and pressure

It is well known that to visually inspect the flow field is one advantage of CFD. The flow field should be consistent with the behaviors of drag and lift forces. Besides, the visualization of the flow field is also an easy way to check whether the overset grid provide smooth interpolation between different blocks of grids. Thus, in this part, snapshots of the flow field at different time instants and Re_d are presented.

A time cycle is chosen to analyze the cyclic behavior of the flow field from the angles of the flow velocity, vorticity structure and the pressure field. The time cycle starts at $\theta = 0$corresponding to a zero lift force and at $\theta = \pi/2$ the lift force increases to its positive maximum. The pressure is presented in the form of the pressure coefficient C_p, which is defined as Eq. (9).

$$C_p = \frac{p}{0.5\rho V_{in}^2} \tag{9}$$

in which, p is the pressure.

Firstly, Figs. 7–9 show the comparisons of the contours of velocity, vorticity and C_p for $\theta = 0$ between "*overset*" and "*noOs*" at $Re_d = 3.15 \times 10^5$. The discrepancies in all three figures are very limited. Moreover, the interpolating errors in the overlap region introduced by the overset grids are not noticeable and the flow field transits "smoothly" between different blocks of grids.

Fig. 10 and Fig. 11 present the contours of the velocity and vorticity by the "*overset*" for $\theta = 0$ at all Reynolds numbers. With the increase of the Reynolds number, the separation of the shear layer is getting more easily observed and the point at which the separation occurs is moving upstream. Moreover, the distributions of the velocity and vorticity are getting more symmetric when Re_d falls into the supercritical regime. The narrowing of wake with Re_d increasing can also be observed.

The behavior of the vortex shedding for a shedding period in "*overset*" cases for $Re_d = 6.31 \times 10^4$ and $Re_d = 7.57 \times 10^5$ are presented in Fig. 12 and Fig. 13. The positive and negative maximum lift coefficients appear when the maximum vorticity value in the wake area is also positive and negative, respectively. It agrees well with the numerical results of other authors [20]. Compared with the flow field at $Re_d = 6.31 \times 10^4$, an earlier separation of the shear layer appears at $Re_d = 7.57 \times 10^5$.

Comparing between Fig. 12 and Fig. 13, the intensity of vorticity is stronger at $Re_d = 6.31 \times 10^4$ than that at $Re_d = 7.57 \times 10^5$. The stronger intensity of vorticity contributes to the larger drag force at $Re_d = 6.31 \times 10^4$. These results can also demonstrate that the overset grid approach combined with the present numerical schemes can well capture some important global flow features in and around the critical flow regime. However, some finer scales of vorticity, especially the instability of the shear layer is not fully captured. It again implies a requirement for other more proper numerical models.

5. Conclusions

An overset grid approach coupled with RANS, *k-ω SST* turbulence model and a set of wall functions are employed to simulate flows around a stationary smooth cylinder. A wide range of Reynolds numbers lying in and around the critical flow regime is investi-

Please cite this article in press as: H. Ye, D. Wan, Benchmark computations for flows around a stationary cylinder with high Reynolds numbers by RANS-overset grid approach, Applied Ocean Research (2017), http://dx.doi.org/10.1016/j.apor.2016.10.010

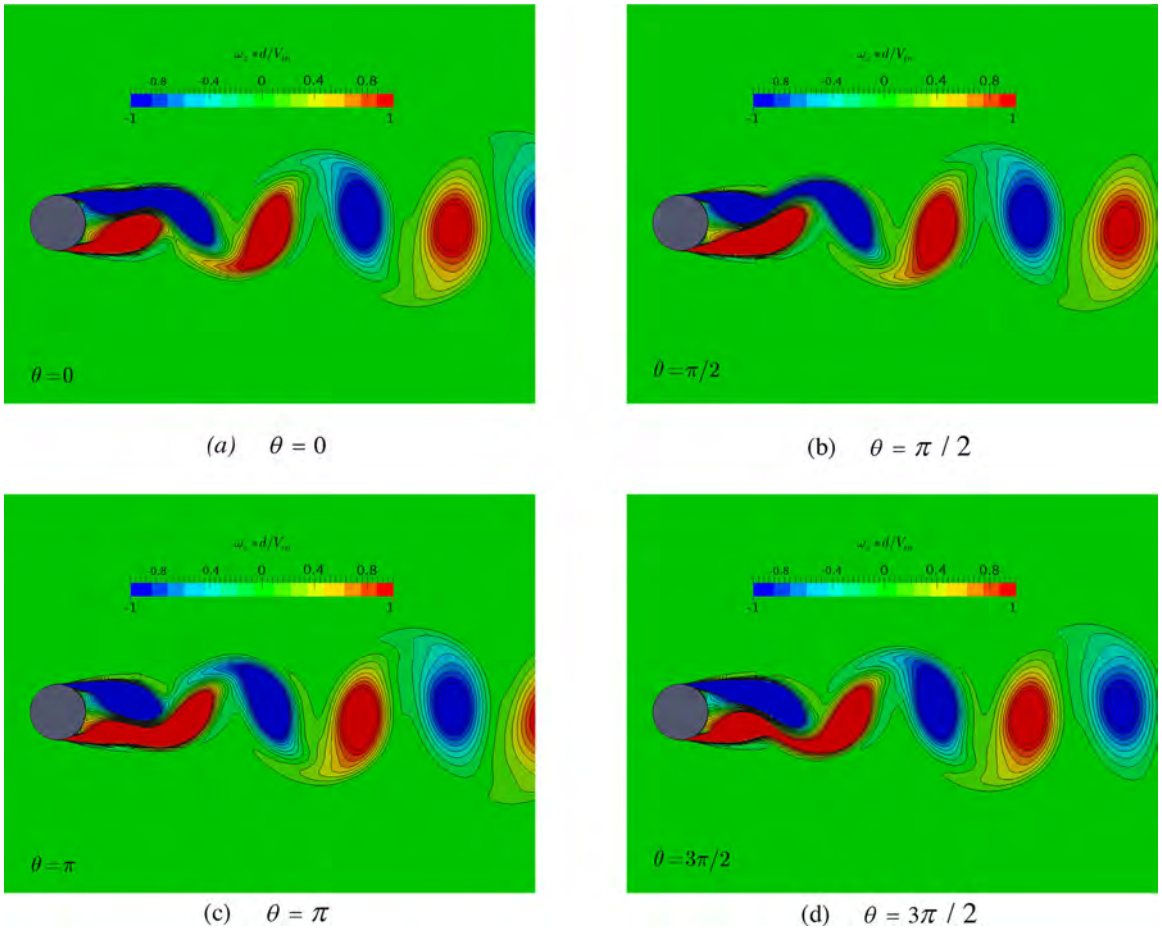

(a) $\theta = 0$ (b) $\theta = \pi / 2$

(c) $\theta = \pi$ (d) $\theta = 3\pi / 2$

Fig. 13. $\omega_z d/V_{in}$ in a vortex-shedding period at $Re_d = 7.57 \times 10^5$ by overset.

gated. The numerical cases both with and without the overset grid approach are carried out. From the comparisons among the present results and the experimental data, several conclusions are carefully drawn:

1. The results of the grid convergence study show that, the present numerical solutions are very sensitive to spatial resolution. The combination of the overset grid approach and *pimpleFoam* has a satisfying stability.
2. As to $C_{L,rms}$, the agreement between the results obtained from "*overset*" and the experiment data is satisfying in the supercritical flow regime. However, a large discrepancy is noted in the subcritical flow regime.
3. The fluctuation of $C_{L,ave}$ is not captured by the present numerical results, which may indicate that *k-ω SST* generates excess eddy viscosity.
4. The results of drag force and *St* demonstrate that the present numerical schemes and models can predict some important trends in the critical flow regime, including the drag crisis and the increase of *St*. However, the present numerical solutions fail to provide an accurate quantitative prediction of the sharp changes.
5. Important global flow features are captured by "*overset*". Whereas, the present numerical solutions are incapable of predicting vorticities and instability of shear layers at a very fine scale. This can directly cause that the flow characteristics in the critical and supercritical flow regimes are not predicted quantitatively.

From the conclusions listed above, it can be seen that the present rudimentary work demonstrates the accuracy, stability and efficiency of the overset grid approach. When the VIV problems are further studied, the quality of the overset grids will not degrade, since any block of the overset grids will not deform as conventional grids. Thus, the overset grid approach can be a more attractive choice if the motions of a cylinder need to be considered. In addition, a real riser usually has strikes making the geometric more complex, which can be easily handled by a set of overset grids.

The present results also expose the inefficiency of RANS combined with *k-ω SST* turbulence model and wall functions in capturing flow features in the critical flow regime. More advanced turbulence models or wall functions can be considered. In the current stage, to implement the overset grid approach with other numerical models provided by OpenFOAM is available, but further verification and validation are still needed.

Acknowledgements

This work is supported by the National Natural Science Foundation of China (51379125, 51490675, 11432009, 51579145), Chang Jiang Scholars Program (T2014099), Program for Professor of Special Appointment (Eastern Scholar) at Shanghai Institutions of Higher Learning (2013022) and Innovative Special Project of Numerical Tank of Ministry of Industry and Information Technology of China (2016-23/09), to which the authors are most grateful. We also thank Prof. Pablo Carrica of University of Iowa for provid-

Please cite this article in press as: H. Ye, D. Wan, Benchmark computations for flows around a stationary cylinder with high Reynolds numbers by RANS-overset grid approach, Applied Ocean Research (2017), http://dx.doi.org/10.1016/j.apor.2016.10.010

ing the overset grid interpolating data which is an indispensable part of this work.

References

[1] A. Trim, H. Braaten, H. Lie, M. Tognarelli, Experimental investigation of vortex-induced vibration of long marine risers, J. Fluids Struct. 21 (2005) 335–361.
[2] G.N. Coleman, R.D. Sandberg. A primer on direct numerical simulation of turbulence-methods procedures and guidelines, 2010.
[3] W. Rodi, Comparison of LES and RANS calculations of the flow around bluff bodies, J. Wind Eng. Ind. Aerodyn. 69 (1997) 55–75.
[4] C. Speziale, Turbulence modeling for time-dependent RANS and VLES: a review, AIAA J. 36 (1998) 173–184.
[5] S. Dong, G.E. Karniadakis, DNS of flow past a stationary and oscillating cylinder at, J. Fluids Struct. 20 (2005) 519–531.
[6] P. Catalano, M. Wang, G. Iaccarino, P. Moin, Numerical simulation of the flow around a circular cylinder at high Reynolds numbers, Int. J. Heat Fluid Flow 24 (2003) 463–469.
[7] M. Saghafian, P. Stansby, M. Saidi, D. Apsley, Simulation of turbulent flows around a circular cylinder using nonlinear eddy-viscosity modelling: steady and oscillatory ambient flows, J. Fluids Struct. 17 (2003) 1213–1236.
[8] E. Guilmineau, P. Queutey, Numerical simulation of vortex-induced vibration of a circular cylinder with low mass-damping in a turbulent flow, J. Fluids Struct. 19 (2004) 449–466.
[9] Z. Pan, W. Cui, Q. Miao, Numerical simulation of vortex-induced vibration of a circular cylinder at low mass-damping using RANS code, J. Fluids Struct. 23 (2007) 23–37.
[10] A. Travin, M. Shur, M. Strelets, P. Spalart, Detached-eddy simulations past a circular cylinder flow, Turbul. Combust. 63 (2000) 293–313.
[11] P.M. Carrica, R.V. Wilson, R.W. Noack, F. Stern, Ship motions using single-phase level set with dynamic overset grids, Comput. Fluids 36 (2007) 1415–1433.
[12] W.D. Henshaw, Overture: an object-oriented framework for overlapping grid applications, AIAA Conference on Applied Aerodynamics (2002).
[13] Z. Shen, D.C. Wan, P. Carrica, Dynamic overset grids in OpenFOAM with application to KCS self-propulsion and maneuvering, Ocean Eng. 108 (2015) 287–306.
[14] D.C. Wan, Z. Shen, Overset-RANS computations of two surface ships moving in viscous fluids, Int. J. Comput. Methods 9 (2012) 1–14, 1240013.
[15] F.R. Menter, Two-equation eddy-viscosity turbulence models for engineering applications, AIAA J. 32 (1994) 1598–1605.
[16] D.C. Wilcox, Turbulence Modeling for CFD, DCW industries, La Canada, CA, 1998.
[17] I. Rodríguez, O. Lehmkuhl, J. Chiva, R. Borrell, A. Oliva, On the flow past a circular cylinder from critical to super-critical Reynolds numbers: wake topology and vortex shedding, Int. J. Heat Fluid Flow 55 (2015) 91–103.
[18] H. Jasak. Error analysis and estimation for the finite volume method with applications to fluid flows. 1996.
[19] S. Patankar, Numerical Heat Transfer and Fluid Flow, CRC Press, 1980.
[20] R.I. Issa, Solution of the implicitly discretised fluid flow equations by operator-splitting, J. Comput. Phys. 62 (1986) 40–65.
[21] J.H. Ferziger, M. Peric, Computational Methods for Fluid Dynamics, Springer Science & Business Media, 2012.
[22] J. De Wilde, R. Huijsmans, Experiments for high Reynolds numbers VIV on risers international society of offshore and polar engineers, The Eleventh International Offshore and Polar Engineering Conference (2001).
[23] E. Furbo, J. Harju, H. Nilsson. Evaluation of turbulence models for prediction of flow separation at a smooth surface Unpublished, 2009.
[24] Z. Shen, H. Ye, D.C. Wan, URANS simulations of ship motion responses in long-crest irregular waves, J. Hydrodyn. 26 (3) (2014) 436–446.
[25] R. Zha, H. Ye, Z. Shen, D.C. Wan, Numerical computations of resistance of high speed catamaran in calm water, J. Hydrodyn. 26 (6) (2014) 930–938.
[26] H. Cao, D.C. Wan, RANS-VOF solver for solitary wave run-up on a circular cylinder, China Ocean Eng. 29 (2) (2015) 183–196.
[27] W. Zhao, D.C. Wan, Numerical investigation of vortex-Induced motions of SPAR platform based on large eddy simulation, Chin. J. Hydrodyn. 30 (1) (2015) 40–46.
[28] Z. Shen, D.C. Wan, An irregular wave generating approach based on naoe-FOAM-SJTU solver, China Ocean Eng. 30 (2) (2016) 177–192.
[29] W. Zhao, D.C. Wan, Numerical study of 3D flow past a circular cylinder at subcritical reynolds number using SST-DES and SST-URANS, Chin. J. Hydrodyn. 31 (1) (2016) 1–8.
[30] W. Zhao, D.C. Wan, R. Sun, Detached-eddy simulation of flows over a circular cylinder at high reynolds number, proceedings of the twenty-sixth (2016), in: International Ocean and Polar Engineering Conference Rhodes, Greece June 26–July 1, 2016, pp. 1074–1079.
[31] W. Zhao, D.C. Wan, Numerical computations of spar vortex-Induced motions at different current headings, in: Proceedings of the Twenty-sixth (2016) International Ocean and Polar Engineering Conference Rhodes, Greece June 26–July 1, 2016, pp. 1122–1127.
[32] M. Duan, D.C. Wan, Frequency and moving direction effects on lift, drag and vortex mode for flows around an oscillating cylinder, in: Proceedings of the Twenty-fifth (2015) International Ocean and Polar Engineering Conference, Kona, Big Island, Hawaii, USA, June 21–26, 2015, pp. 1010–1017.
[33] M. Duan, D.C. Wan, H. Xue, Prediction of response for vortex-induced vibrations of a flexible riser pipe by using multi-strip method, in: Proceedings of the Twenty-sixth (2016) International Ocean and Polar Engineering Conference Rhodes, Greece June 26–July 1, 2016, pp. 1065–1073.

Please cite this article in press as: H. Ye, D. Wan, Benchmark computations for flows around a stationary cylinder with high Reynolds numbers by RANS-overset grid approach, Applied Ocean Research (2017), http://dx.doi.org/10.1016/j.apor.2016.10.010